ENVIRONMENTAL RESEARCH
LETTERS

PURPOSE-LED PUBLISHING™

LETTER • OPEN ACCESS

Modulation of western North Pacific tropical cyclone decadal variability by the Victoria mode

To cite this article: Tao Wen *et al* 2025 *Environ. Res. Lett.* **20** 034003

View the article online for updates and enhancements.

You may also like

- Hybrid combination of advanced oxidation process with membrane technology for wastewater treatment: gains and problems
Chhabilal Regmi, Yuwaraj K Kshetri and S Ranil Wickramasinghe
- Gaps in U.S. livestock data are a barrier to effective environmental and disease management
Rebecca Logsdon Muenich, Sanskriti Aryal, Amanda J Ashworth et al.
- Effects of composition ratio and crystal orientation on nanoindentation behavior of monocrystal AuPt alloys
Jiajun Lin, Hao Xu, Yuanyuan Tian et al.

This content was downloaded from IP address 223.81.87.228 on 16/02/2025 at 03:11

ENVIRONMENTAL RESEARCH
LETTERS

OPEN ACCESS

RECEIVED
21 October 2024

REVISED
30 December 2024

ACCEPTED FOR PUBLICATION
30 January 2025

PUBLISHED
11 February 2025

Original content from this work may be used under the terms of the Creative Commons Attribution 4.0 licence.

Any further distribution of this work must maintain attribution to the author(s) and the title of the work, journal citation and DOI.

LETTER

Modulation of western North Pacific tropical cyclone decadal variability by the Victoria mode

Tao Wen[1,2], **Jianping Li**[3,4], **Shifei Tu**[5], **Ruiqiang Ding**[1,2,*], **Quanjia Zhong**[6,*] and **Xumin Li**[1,2]

[1] State Key Laboratory of Earth Surface Processes and Hazards Risk Governance (ESPHR), Faculty of Geographical Science, Beijing Normal University, Beijing, People's Republic of China
[2] Key Laboratory of Environmental Change and Natural Disasters of Chinese Ministry of Education/Faculty of Geographical Science, Beijing Normal University, Beijing, People's Republic of China
[3] Key Laboratory of Physical Oceanography-Institute for Advanced Ocean Studies, Qingdao National Laboratory for Marine Science and Technology, Ocean University of China, Qingdao, People's Republic of China
[4] Laoshan Laboratory, Qingdao, People's Republic of China
[5] South China Sea Institute of Marine Meteorology/College of Ocean and Meteorology, Guangdong Ocean University, Zhanjiang, People's Republic of China
[6] Center for Ocean Research in Hong Kong and Macau, Department of Ocean Science, The Hong Kong University of Science and Technology, Hong Kong Special Administrative Region of China, People's Republic of China
[*] Authors to whom any correspondence should be addressed.

E-mail: drq@bnu.edu.cn and zqj@lasg.iap.ac.cn

Keywords: North Pacific, tropical cyclone, decadal, variability

Supplementary material for this article is available online

Abstract

Intense tropical cyclones (TCs) in the southeastern western North Pacific (SE-WNP) significantly impact East Asian coastal nations. Decadal variability in TC genesis frequency (TCGF) has been linked to the Pacific decadal oscillation (PDO), a major sea surface temperature (SST) pattern in the North Pacific. However, based on extended observation records, we show that the decadal variability of SE-WNP TCGF is mainly driven by the Victoria mode (VM), a secondary but prominent SST pattern in the North Pacific. During the positive VM phase, the SE-WNP TCGF is more than usual due to the anomalous large-scale environmental fields induced by the VM-related central North Pacific SST anomalies; conversely, the SE-WNP TCGF is less during the negative VM phase. This highlights the crucial role of the VM in modulating TC activity, challenging the traditional view that the PDO is the dominant factor, with important implications for SE-WNP TC climate predictions.

1. Introduction

Tropical cyclones (TCs) cause significant loss of life and severe economic damage, making them one of the world's most devastating natural disasters. (Murnane and Elsner 2012, Kunze 2021). The western North Pacific (WNP) is home to nearly one-third of TCs annually (Chan 1985, Guo and Tan 2018), making it the most active basin globally (Zhan *et al* 2022). In particular, nearly 80% of the most intense TCs, which account for nearly half of economic losses and numerous casualties in East Asian coastal nations, originate in the southeastern part of the WNP (SE-WNP; Kunze 2021, Huang *et al* 2022). Therefore, a better understanding of TC variability over the SE-WNP is essential.

The SE-WNP TC genesis frequency (TCGF) shows significant decadal variability. Previous investigations suggested that SE-WNP TCGF decadal variability is primarily modulated by the Pacific decadal oscillation (PDO) or Interdecadal Pacific oscillation (IPO; Zhao *et al* 2018, Zhou *et al* 2024), the most prominent sea surface temperature (SST) variability in the Pacific with a long-term fluctuation on the decadal time scale (Mantua *et al* 1997, Matua and Hare 2002). However, these studies suggested that this variability is primarily influenced by the PDO/IPO for the SE-WNP TCGF decadal variability are based on data since the late 1970s (Zhao *et al* 2018, Liu *et al* 2019). This timeframe may be insufficient to accurately assess the connection between the SE-WNP TCGF decadal variability and PDO/IPO.

© 2025 The Author(s). Published by IOP Publishing Ltd

Here we show that there is only a weak relationship between decadal variability of SE-WNP TCGF and PDO/IPO when using data extending back to the 1950s; instead, there is a significant and stable relationship of the SE-WNP TCGF decadal variability with the Victoria mode (VM), the second most influential SST pattern in the North Pacific (Ding *et al* 2015, Ji *et al* 2023). Previous studies have shown that the VM exerts a modulating effect on WNP TCGF on the interannual scale (Pu *et al* 2019), but our study highlights the importance of the VM in modulating SE-WNP TCGF decadal variability.

2. Results

2.1. Relationship between decadal variability of SE-WNP TCGF and VM

We first showed the decadal components (spanning periods greater than 11 years) of the VM index during boreal spring (February–April; FMA; the peak season of the VM; Ding *et al* 2018) and the following typhoon seasons (June–October; JJASO) averaged SE-WNP TCGF and PDO index (see Methods; denoted as the VM_LF, TC_LF, and PDO_LF, respectively) for the period 1950–2022 (figure 1(a)). The contributions of the inter-decadal variability of the VM and TCGF to their respective variances, which are 25% and 41% respectively. Particularly, the contribution of the inter-decadal component to the VM variability shows an upward trend (Ji *et al* 2024). The VM_LF shows a strong correlation with the TC_LF over the entire period ($R = 0.75$, statistically significant at the 0.05 level). In contrast, the correlation between the simultaneous PDO_LF and TC_LF is much weaker ($R = 0.31$).

We calculated the sliding correlations of the VM_LF and PDO_LF respectively with the TC_LF on a 23 year moving window (figure 1(b)). The VM − TC relationship shows a significant positive correlation over almost the entire period. In contrast, the PDO − TC relationship shows an abrupt shift in the late 1980s (Zhou *et al* 2024), with significant positive correlations from 1986–2022 (P2), but no such correlation before 1986 (P1;1950–1985). The above results are stable across different lengths of the moving window (supplementary figure 1).

We next adopt the dynamic genesis potential index (DGPI), which integrates the effects of dynamic parameters and shows a positive ability to depict the decadal variation of the number of TCs over the WNP (see Methods; Zhan *et al* 2022). The decadal components of DGPI and TC_LF over the SE-WNP have a strong positive correlation ($R = 0.66$, with a 95% confidence level) for the period 1950–2022 (supplementary figure 2). The spatial correlations of JJASO DGPI respectively with the FMA VM index and the JJASO PDO index show that significant positive correlations with the VM index covers over most of the SE-WNP, while only weak correlations are observed with the PDO index over the SE-WNP (supplementary figure 3). These observational results suggest that decadal variability of SE-WNP TCGF may be controlled by the VM, but not by the PDO.

Given that the SE-WNP is the main genesis region for super TCs ($\geqslant$51.0 m s^{-1}; Huang *et al* 2022), the VM could therefore modulate the genesis frequency of super TCs by controlling the genesis frequency of all TCs in this region. It shows that there is a much higher genesis frequency of TCs over the SE-WNP during positive VM events than during negative VM events (72% vs 28%; figure 2(a)). Furthermore, 81% of super TCs originating from the SE-WNP occur during positive VM years, while only 19% of super TCs occur during negative VM years (figure 2(b)). In contrast, there is no obvious difference in the genesis frequency of all TCs and super TCs between positive and negative PDO (supplementary figure 4). This finding is very important for climate prediction of super TCs over the SE-WNP.

The role of the VM in controlling SE-WNP TCGF decadal variability is also supported by CMIP6 models (supplementary table 1; see 'Methods' for model selections). A total of 12 out of the selected 15 models (80%) show that the correlation coefficient of decadal variability of the JJASO DGPI over the SE-WNP with the FMA VM is higher than that with the JJASO PDO, while only 3 out of the 15 models exhibit the opposite inclination (figure 3(a)). The results from the AMIP6 experiments show similar findings, with 24 out of the 25 models indicating that the JJASO DGPI over the SE-WNP is greater during positive VM events than negative ones. (supplementary figure 5).

Two sets of ensemble experiments using the Community Earth System Model (CESM) show that the FMA VM can indeed affect the subsequent JJASO SE-WNP TCGF (see Methods). In the positive-VM ensemble run, a high area-averaged JJASO DGPI is shown over the SE-WNP. In contrast, in the negative-VM ensemble run, the JJASO DGPI over SE-WNP is low (figure 3(b)). The difference is statistically significant at the 95% confidence level, based on the bootstrap method (see methods). These modeling results further indicate that the VM plays a crucial role in controlling the decadal variability of SE-WNP TCGF.

2.2. Physical mechanisms driving the VM's modulation effect

We have shown that the VM may be an important factor in controlling the decadal variability of SE-WNP TCGF. We next investigate the mechanisms through which the VM controls the decadal variability of SE-WNP TCGF. Previous studies have demonstrated that the central North Pacific (CNP; 0–20° N, 160° E–160° W) is a key region influencing the variability of SE-WNP TCGF (Zhou *et al* 2024). The VM is associated with a tripole SSTAs pattern in the North Pacific from FMA to summer, driven by

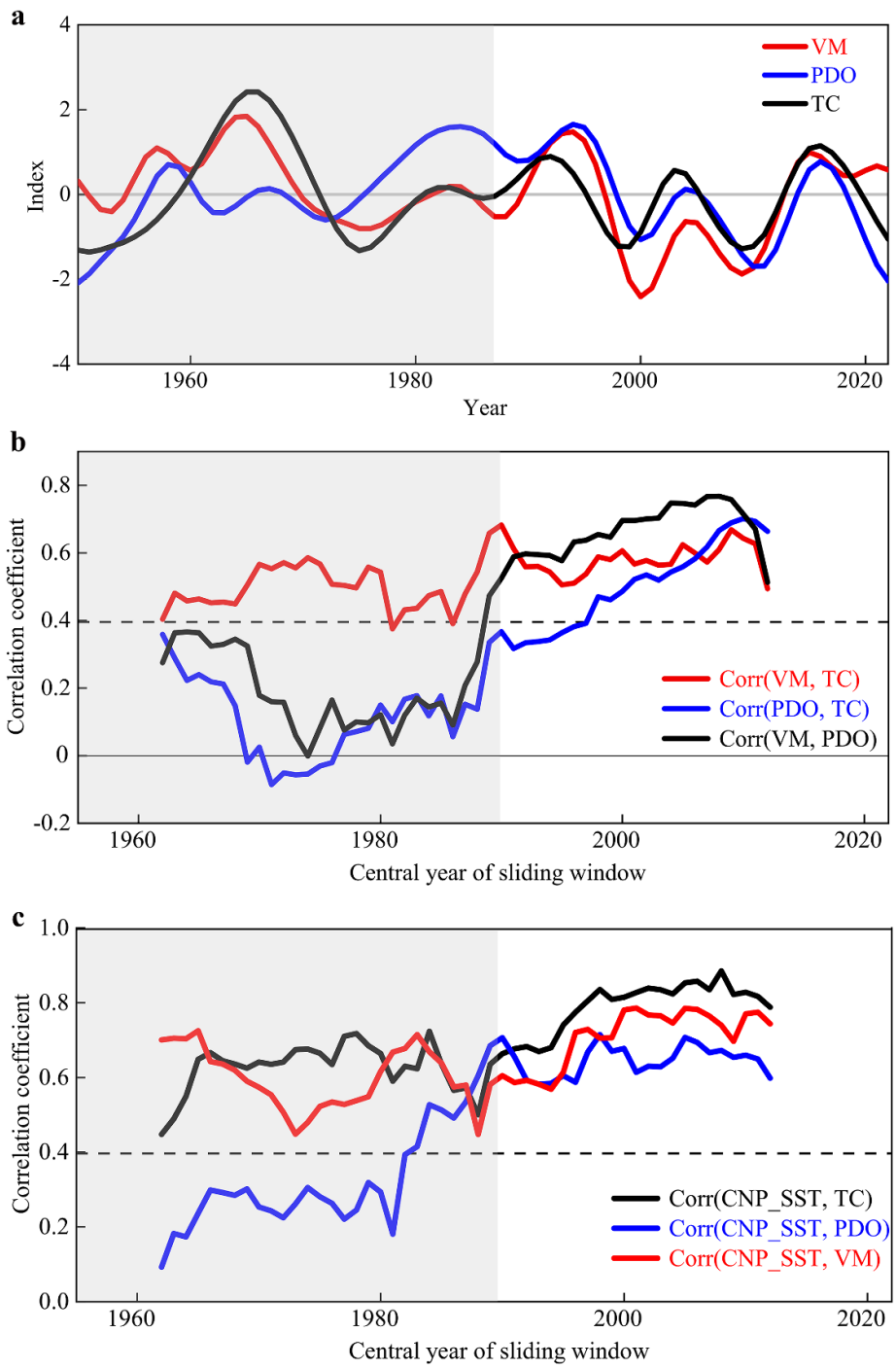

Figure 1. Relationships of the VM and PDO with decadal variability of SE-WNP TCGF in observations. (a) Time evolutions of the PDO-LF (blue line), VM_LF (red line), and SE-WNP TC_LF (black line). (b) The 23 year sliding correlations of the VM_LF and PDO_LF respectively with the TC_LF, and the 23 year sliding correlations of the VM_LF with the PDO_LF. (c) The 23 year sliding correlations of the TC_LF, VM_LF and PDO_LF respectively with the CNP SST index. The horizontal dashed lines in (b) and (c) denote the 95% confidence levels based on the two-tailed Student's test. The grey shaded areas in (a)–(c) indicate the first period (P1; 1950–1985).

a lagged ocean-air coupling process, such as wind-evaporation-SST feedback (Xie *et al* 1994, Ding *et al* 2018). This process can then force the overlying atmosphere to initiate CNP SST anomalies, an evolving process known as the seasonal footprinting mechanism (Vimont *et al* 2003). Overall, the lagged ocean-air response of CNP-SST anomalies to VM is more stable and has a more significant during the whole period (figure 1(c)). However, the PDO-related ocean-air process has an unstable effect on the CNP-SST, and it is significant only during the P2 period, with a poorer relationship during the P1 period.

There is a strong positive correlation coefficient between the JJASO TC_LF and the simultaneous CNP SST index (see methods) for the entire period (R = 0.68, with a 95% confidence level;

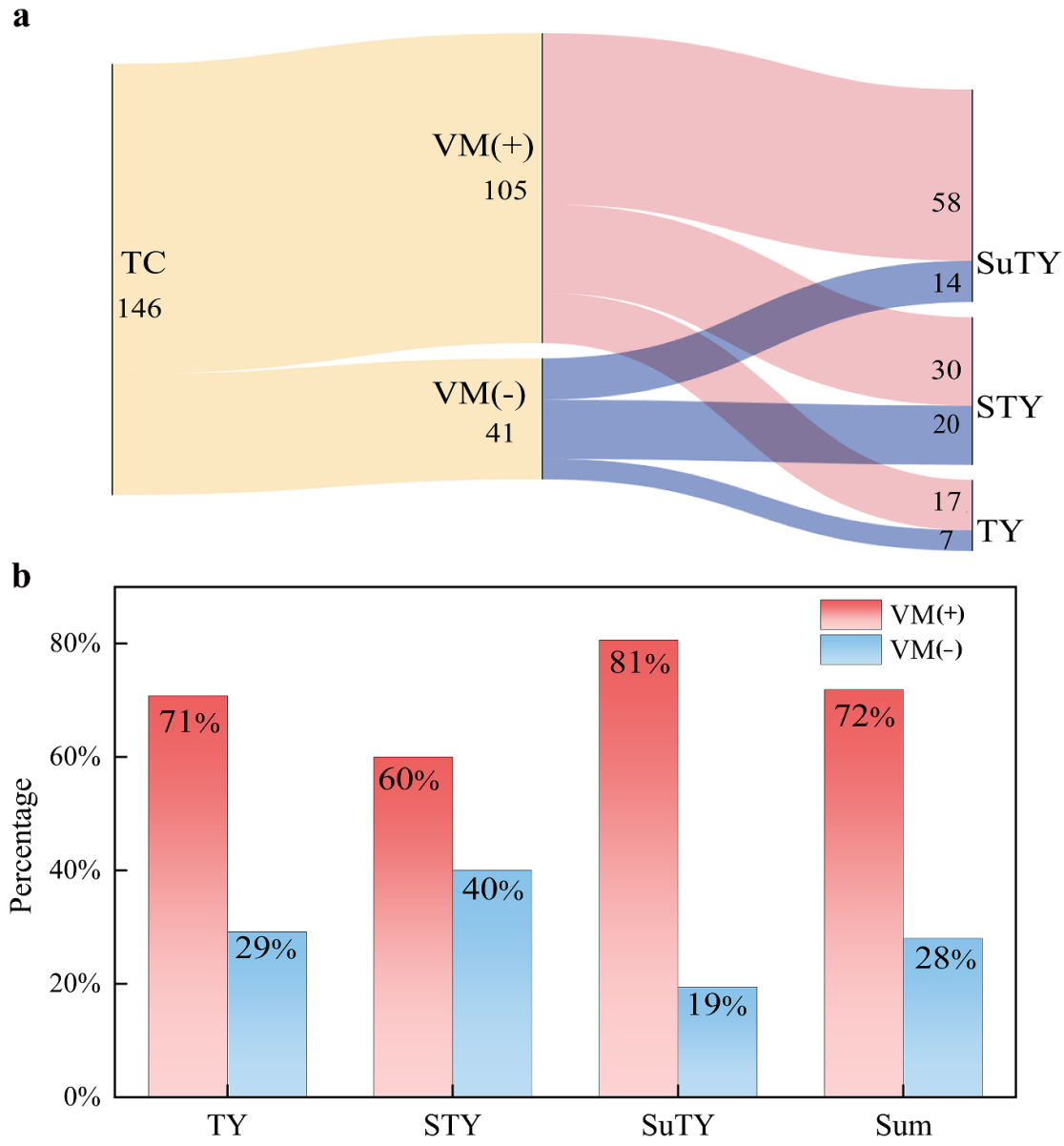

Figure 2. Difference in SE-WNP TCGF between positive and negative VM events. (a) Sankey diagram showing the flow of different TC intensities (SuTY, STY, TY) over the SE-WNP for positive/negative VM events. Number of TCs is listed at the center of each set of diagrams. Line widths are proportional to the magnitude of the corresponding flow. Super typhoon (SuTY; $\geqslant$51.0 m s^{-1}), strong typhoon (STY; 41.5–50.9 m s^{-1}), typhoon (TY; 32.7–41.4 m s^{-1}), defined by the maximum TC wind speed, are shown to the far right of the flow line. (b) Comparison of the percentage of SE-WNP TCs with different intensities under positive VM events (red bars) and negative VM events (blue bars). Proportion of TCs are listed at the top of each set of bars.

supplementary figure 6(a)). Furthermore, we note that the relationship between the CNP SST index and SE-WNP TCGF shows a significant and stable positive correlation over almost the entire period (figure 1(c)). After removing the CNP SST index from the VM index, the correlation between the FMA VM and the following JJASO TC_LF drops from 0.75 to 0.33 (supplementary figure 6(a)), and there is no longer a significant and stable relationship between the VM and SE-WNP TCGF (supplementary figure 6(b)). These results indicate that the CNP SST likely plays a crucial role in mediating the influence of the VM on the SE-WNP TC genesis, in line with Liu *et al* (2019).

We show the regressed 850 hPa vorticity, omega, 700 hPa specific humidity, and vertical wind shear (VWS) between 200- and 850 hPa with respect to the CNP SST index (supplementary figure 7). In response to the anomalous CNP SST, cyclonic vorticity anomalies dominate the lower troposphere over the main SE-WNP TC genesis region (supplementary figure 7(a)) and the increased specific humidity (supplementary figure 7(b)), and the middle low troposphere is associated with anomalous ascending motion (supplementary figure 7(c)). Additionally, the VWS is weakened in the region north of the equator and east of 150° E (supplementary figure 7(d)). The combination of these thermodynamic and dynamic conditions favors the genesis of SE-WNP TCs.

Given that the CNP SSTs are closely connected to the variability of SE-WNP TCGF, one question

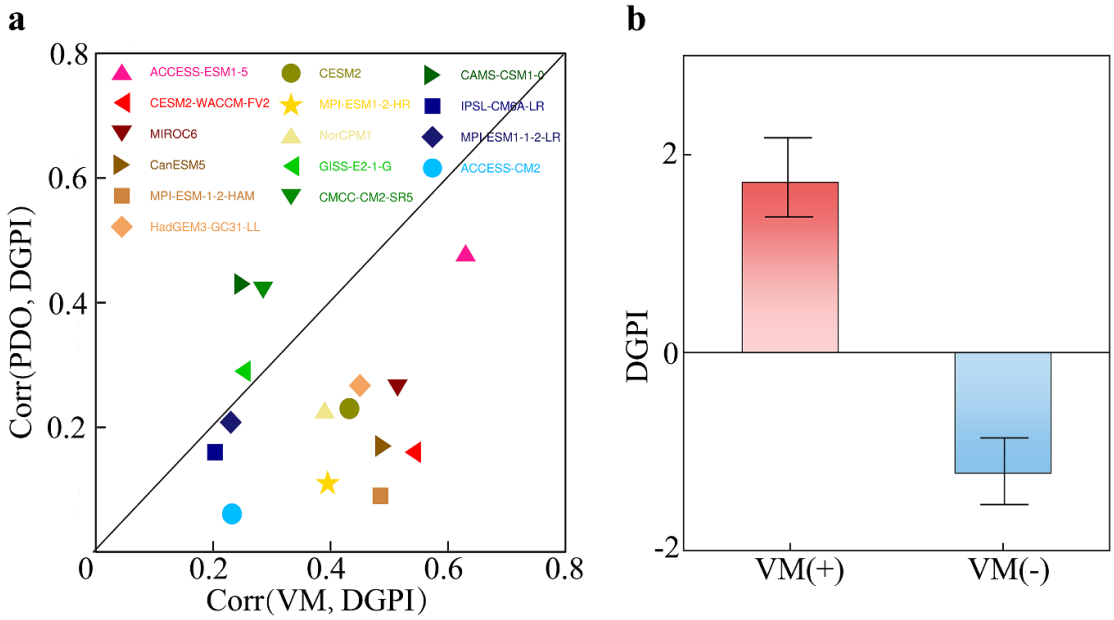

Figure 3. Decadal variability of DGPI over the SE-WNP: inter-model relationships and VM forcing impacts. (a) Inter-model relationship between the correlation coefficient of the decadal variability of the JJASO DGPI over the SE-WNP with the FMA VM and the JJASO PDO. (b) DGPI area-averaged over the SE-WNP induced by positive and negative VM SST forgings by using the CESM. The solid line in (a) is the diagonal, the bottom right of which indicates that the correlation coefficient between the VM and DGPI is greater than that between the PDO and DGPI. Error bars in (b) indicate the 95% confidence intervals.

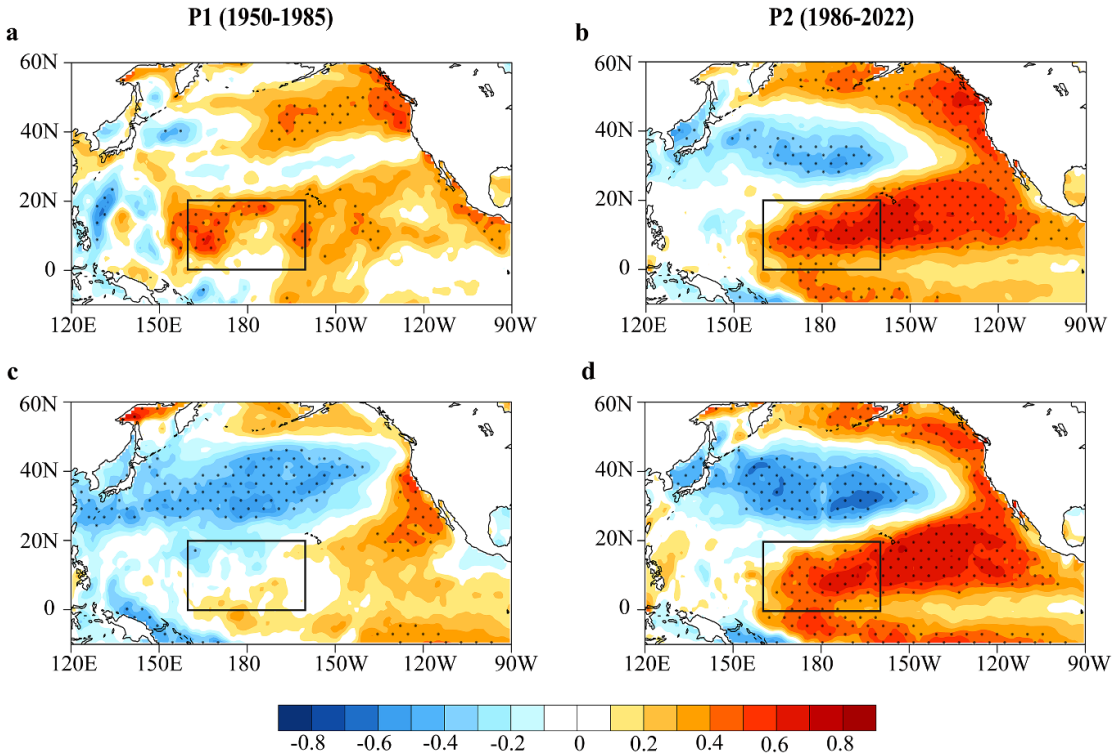

Figure 4. Correlations of the VM and PDO respectively with SSTs in the North Pacific. (a) The spatial correlations of JJASO SSTs with the FMA VM index in the P1 period (1950–1985). (b) Same as (a), but for the P2 period (1986–2022). (c) The spatial correlations of JJASO SSTs with the JJASO PDO index in the P1 period (1950–1985). (d) Same as (c), but for the P2 period. Dots represent correlations statistically significant above the 95% confidence level. Boxes in (a–d) indicate the CNP region (0–20° N, 160° E–160° W).

naturally arises as to why the VM relates well to the SE-WNP TCGF in both the P1 and P2 periods, while the PDO relates well to the SE-WNP TCGF only in the P2 period. We next examined changes in the spatial correlations of JJASO SSTs with the FMA VM index and the JJASO PDO index, respectively (figure 4).

We find that the PDO has significant positive correlations over the CNP region only in the P2 period, which coincides well with the enhanced relationship between the PDO and SE-WNP TCGF during the same period. (figures 4(c) and (d)). The connection between the JJASO CNP SST index and the simultaneous PDO index reaches statistical significance in the P2 period, but no significant correlations in the P1 period (figure 1(c)). In contrast, the VM has significant positive correlations over the CNP region in both the P1 and P2 periods (figures 4(a) and (b)), and the connection between the FMA VM index and the following JJASO CNP SST index remains robust over almost the entire period (figure 1(c)). In particular, from the P1 period to the P2 period, the connection between the VM and CNP SST shows a strengthened trend, which coincides well with the enhanced relationship between the VM and SE-WNP TCGF. Alternatively, the spatial distribution characteristics of the atmospheric environmental fields obtained through the FMA VM_LF regression closely resemble those of the CNP SST index (supplementary figure 8). These results may explain why the VM − TC relationship is significant over almost the entire period, while the PDO − TC relationship is significant only in the P2 period.

Previous studies have shown that the VM-related North Pacific SST anomalies peak in spring and propagate towards the equatorial Pacific through subtropical air–sea feedback processes, initiating the development of ENSO (Bond *et al* 2003, Ding *et al* 2015). During the typhoon season, significant ENSO-like SST anomaly patterns associated with the VM emerge in the central equatorial Pacific, which can project onto the PDO pattern in the North Pacific (Di Lorenzo *et al* 2010). Thus, while the PDO and VM are independent of each other at any given moment, there may be a lagged connection between them (Lorenzo *et al* 2023). As the northeast trade winds strengthen in the subtropical Northeast Pacific in recent decades (Boisséson *et al* 2014), the coupling between the extratropics and tropics tends to enhance (Cai *et al* 2018, Jia *et al* 2021), leading to a stronger lagged linkage between the spring VM and the subsequent summer PDO in the P2 period (Ji *et al* 2024, figure 1(b)). After removing the FMA VM_LF from the JJASO PDO_LF, the correlation between the PDO and SE-WNP TCGF drops from 0.68 to 0.26 in the P2 period (supplementary figure 9). This implies that the close relationship between the PDO and SE-WNP TCGF in the P2 period may simply be a consequence of the enhanced lagged linkage between the VM and PDO (figure 1(b)). This may explain why the PDO relates well to the SE-WNP TCGF only in the P2 period. From this perspective, it is further illustrated that decadal variability of SE-WNP TCGF may be mainly driven by the VM, but not by the PDO.

3. Discussion

We have shown that the decadal variability of SE-WNP TCGF is primarily driven by the VM, but not by the PDO. During the positive VM phase, the SE-WNP TCGF is more than usual due to the anomalous large-scale environmental fields induced by the VM-related CNP SST anomalies; conversely, the SE-WNP TCGF is less during the negative VM phase. These results challenge previous studies by attributing the decadal TC activity over the SE-WNP to the VM rather than the PDO. This finding has significant implications for the long-term prediction of SE-WNP TCs and for enhancing disaster prevention strategies against TC impacts in East Asian coastal nations.

Studies indicate that while the earlier data may have some inconsistencies (Kossin *et al* 2013), the overall trends and patterns observed in the data remain valid for understanding long-term climate changes and cyclone behavior (Chan and Liu 2022, Zhou *et al* 2024) although this still deserves to be verified in further high-resolution model simulations. Foremove, recent study has shown that the variability of the VM has increased in recent decades (Ji *et al* 2024), which may explain a stronger relationship between the VM and SE-WNP TCGF in the P2 period than in the P1 period (figure 1(b)). As the VM tends to intensify in the future, its potential impact on SE-WNP TCs may be also expected to strengthen. In this regard, further investigations are required to examine the relationship between the VM and SE-WNP TCGF in a warming climate.

4. Methods

4.1. Observed data

We used data from multi-species observation and reanalysis datasets, including monthly mean SST from the Hadley Centre global sea ice and SST data (Rayner *et al* 2006), as well as omega, u-wind, v-wind data from the NCEP-NCAR reanalysis (Kalnay *et al* 1996). TC best-track data were obtained from the CMA/China Meteorological Data Service Center (Ying *et al* 2014, Lu *et al* 2021). A TC is considered to occur when the maximum sustained wind speed reaches the critical value of 32.7 m s^{-1}. In this paper, we focus on the season when TC is active (June to October). However, we also use other typhoon seasons such as July to November and the conclusions are unchanged (not shown). Prior to analysis, we remove the linear trends and seasonal cycles from the observed data.

4.2. CMIP6 data

For the model datasets, we used the monthly historical simulations produced by 31 models participating in the CMIP6 (Eyring *et al* 2016). From the 31

models, we selected 15 models for further investigation based on their ability to reproduce the patterns and variability of the VM and PDO (supplementary figure 10). The selected models demonstrate robust performance in both exponential intensity simulation and pattern spatial correlation simulation, aligning with the findings reported by Wang *et al* (2021). The main details of the 15 selected models are summarized in Table 1. For the analysis, we focused on the common period from January 1900 to December 2000. All model data were bilinearly interpolated onto a 1° × 1° latitude and longitude grid for the multi-model ensemble mean analysis.

4.3. Coupled general circulation model (CGCM)

We set a CGCM experiment to run with the CESM version 1.2.2.1 (hereafter CESM; Hurrell *et al* 2013). The CESM is an advanced, fully coupled global climate model developed by NCAR to simulate the Earth system. It integrates various components, including the atmosphere, ocean, land surface, ice, and more. The atmospheric part of CESM is represented by the Community Atmosphere Model version 5, which operates with a horizontal resolution of approximately 1° (1.25° × 0.9°) and 30 vertical layers, and its ocean component is the ParallelOcean Program version 2, which shares a similar horizontal resolution and includes 60 vertical layers. CESM's land and sea ice models are the Community Land Model version 4 and the Los Alamos Sea Ice Model version 4 (CICE4), respectively. This experiment was conducted in two stages. Initially, the CESM was allowed to run freely for 120 years under preindustrial (1850) radiative forcing conditions, referred to as the CTRL simulation. In the second stage, we performed sensitivity experiments with both positive and negative VM simulations, each consisting of 30 ensemble members. The SSTs during February–April over the North Pacific (0–60° N, 100° E–100° W) is nudged toward SSTAs associated with the positive or negative VM, in addition to the climatological SSTs. These VM-related SSTAs were derived by regressing the corresponding 2 × SSTAs onto the FMA VMI.

Each ensemble member was integrated from January to February of the second year, resulting in a total integration period of 14 months.

4.4. Climate indices

The PDO and VM indices are represented by the principal component time series of the first and second dominant empirical orthogonal function of monthly SST anomalies over the extratropical North Pacific (20°–65° N, 124° E–100° W) for the period 1950–2022 (Mantua and Hare 2002, Bond *et al* 2003). The VM was analyzed during its peak season (FMA). For the PDO, we selected the JJASO (June–October) season to align with the established typhoon season, ensuring consistency with previous research (Liu *et al* 2019, Zhan *et al* 2022). Additionally, we examined the PDO across different seasons, confirming that our conclusions remain independent of the specific PDO season chosen (supplementary figure 11).

The DGPI is calculated using the method outlined in Wang *et al* (2020). It is given by:

$$\mathrm{DGPI} = (2+0.1V_s)^{-1.7}\left(5.5-\frac{\mathrm{d}u}{\mathrm{d}y}10^5\right)^{2.3} \times (5-20w)^{3.3}\left(5.5+\left|10^5\eta\right|\right)^{2.4}\mathrm{e}^{-11.8}-1.$$

Here, V_s represents the magnitude of VWS between 200 and 850 hPa, du/dy is the meridional gradient of zonal wind at 500 hPa, w denotes the 500 hPa vertical pressure velocity, and η is absolute the at 850 hPa.

The CNP SST indices represent the area-averaged SSTAs over the CNP region (0–20° N, 160° E–160° W). The manuscript applied an 11-point Lanczos low-pass filter to extract the decadal variability of all climate indices and variables. All indices have been detrended before analysis.

4.5. Positive and negative VM/PDO events

We categorize VM events from the period 1950–2022 based on the magnitude of the three-month average FMA VMI. Years in which this index equals or exceeds one standard deviation during spring are classified as positive VM events years. Conversely, years in which the index is less than to negative one standard deviation are classified as negative VM events years. Likewise, we categorize PDO events from 1950–2022 based on the average JJASO PDO index for the typhoon season. Years with a PDO index of ±1 standard deviation are classified as positive or negative PDO events, respectively.

4.6. Significance tests

Statistical significance of correlations and regressions was assessed using a two-tailed Student's t-test. Since the number of yearly TCs follows a Poisson distribution (Ji *et al* 2024), we applied a non-parametric bootstrap method to test the significance of genesis and track density differences between periods. This method, commonly used in climate research, is suitable for small sample sizes and makes no assumption about the underlying statistical distribution (Tippett *et al* 2011). The effective sample size was adjusted as described by Li *et al* (2013) when testing linear correlations. Additionally, we used bootstrapping (Austin and Tu 2004) to examine whether the area-averaged JJASO DGPI connections differed significantly between positive and negative VM phases.

Data availability statement

The HadISST dataset, TC best-track data and NCEP-NCAR Reanalysis data can be available at

www.metoffice.gov.uk/hadobs/hadsst3/, https://g.hyyb.org/systems/TY/info/tcdataCMA/zjljsjj_zlhq.html, https://psl.noaa.gov/data/gridded/data.ncep.reanalysis.html, respectively.

Acknowledgment

This research was jointly supported by the National Natural Science Foundation of China (42225501, 42105059), and China's National Key Research and Development Projects (2020YFA0608400).

Code availability statement

The data in this study were analyzed with NCAR Command Language (NCL; http://dx.doi.org/10.5065/D6WD3XH5). All relevant codes used in this study are available, upon request, from the corresponding authors R Q D and Q J Z.

Author contributions

R Q D and T W designed the study. T W wrote the paper and performed the data analysis and prepared all figures. X M L conducted the modelling experiments. R Q D and Q J Z contributed to the interpretation of the results and the improvement of the manuscript.

Conflict of interest

The authors declare no competing interests.

ORCID iDs

Tao Wen https://orcid.org/0000-0001-9433-3452
Jianping Li https://orcid.org/0000-0003-0625-1575
Ruiqiang Ding https://orcid.org/0000-0003-4139-3843
Quanjia Zhong https://orcid.org/0000-0002-6774-3146

References

Austin P C and Tu J V 2004 Bootstrap methods for developing predictive models *Am. Stat.* **58** 131–7
Bond N A, Overland J E, Spillane M and Stabeno P 2003 Recent shifts in the state of the North Pacific *Geophys. Res. Lett.* **30** 2183
Cai W *et al* 2018 Increased variability of eastern Pacific El Niño under greenhouse warming *Nature* **564** 201–6
Chan J C L 1985 Tropical cyclone activity in the Northwest Pacific in relation to the El Niño/Southern oscillation phenomenon *Mon. Weather Rev.* **113** 599–606
Chan J C L and Liu K S 2022 Recent decrease in the difference in tropical cyclone occurrence between the Atlantic and the Western North Pacific *Adv. Atmos. Sci.* **39** 1387–97
de Boisséson E, Balmaseda M A, Abdalla S, Källén E and Janssen P A E M 2014 How robust is the recent strengthening of the tropical Pacific trade winds? *Geophys. Res. Lett.* **41** 4398–405
Di Lorenzo E, Cobb K M, Furtado J C, Schneider N, Anderson B T, Bracco A, Alexander M A and Vimont D J 2010 Central Pacific El Niño and decadal climate change in the North Pacific Ocean *Nat. Geosci.* **3** 762–5
Ding R, Li J, Tseng Y H, Sun C and Guo Y 2015 The Victoria mode in the North Pacific linking extratropical sea level pressure variations to ENSO *J. Geophys. Res. Atmos.* **120** 27–45
Ding R, Li J, Tseng Y-H, Li L, Sun C and Xie F 2018 Influences of the North Pacific Victoria mode on the South China Sea summer monsoon *Atmosphere* **9** 229
Eyring V, Bony S, Meehl G A, Senior C A, Stevens B, Stouffer R J and Taylor K E 2016 Overview of the coupled model intercomparison project phase 6 (CMIP6) experimental design and organization *Geosci. Model Dev.* **9** 1937–58
Guo Y-P and Tan Z-M 2018 Westward migration of tropical cyclone rapid-intensification over the Northwestern Pacific during short duration El Niño *Nat. Commun.* **9** 1507
Huang M *et al* 2022 Increasing typhoon impact and economic losses due to anthropogenic warming in Southeast China *Sci. Rep.* **12** 14048
Hurrell J W *et al* 2013 The community earth system model: a framework for collaborative research *Bull. Am. Meteorol. Soc.* **94** 1339–60
Ji K, Tseng Y, Ding R, Mao J and Feng L 2023 Relative contributions to ENSO of the seasonal footprinting and trade wind charging mechanisms associated with the Victoria mode *Clim. Dyn.* **60** 47–63
Ji K, Yu J-Y, Li J, Hu Z-Z, Tseng Y-H, Shi J, Zhao Y, Sun C and Ding R 2024 Enhanced North Pacific Victoria mode in a warming climate *npj Clim. Atmos. Sci.* **7** 49
Jia F, Cai W, Gan B, Wu L and Di Lorenzo E 2021 Enhanced North Pacific impact on El Niño/Southern oscillation under greenhouse warming *Nat. Clim. Change* **11** 840–7
Kalnay E *et al* 1996 NCNP/NCAR 40-year reanalysis project *Bull. Am. Meteorol. Soc.* **77** 437–72
Kossin J P, Olander T L and Knapp K R 2013 Trend analysis with a new global record of tropical cyclone intensity *J. Clim.* **26** 9960–76
Kunze S 2021 Unraveling the effects of tropical cyclones on economic sectors worldwide: direct and indirect impacts *Environ. Resour. Econ.* **78** 545–69
Li J, Sun C and Jin F-F 2013 NAO implicated as a predictor of Northern Hemisphere mean temperature multidecadal variability *Geophys. Res. Lett.* **40** 5497–502
Liu C, Zhang W, Stuecker M F and Jin F-F 2019 Pacific meridional mode-Western North Pacific tropical cyclone linkage explained by tropical Pacific quasi-decadal variability *Geophys. Res. Lett.* **46** 13346–54
Lorenzo E D *et al* 2023 Modes and mechanisms of Pacific decadal-scale variability *Annu. Rev. Mar. Sci.* **15** 249–75
Lu X *et al* 2021 Western North Pacific tropical cyclone database created by the China meteorological administration *Adv. Atmos. Sci.* **38** 690–9
Mantua N J, Hare S R, Zhang Y, Wallace J M and Francis R C 1997 A Pacific interdecadal climate oscillation with impacts on salmon production *Bull. Am. Meteorol. Soc.* **78** 1069
Mantua N J and Hare S R 2002 The Pacific decadal oscillation *J. Oceanogr.* **58** 35–44
Murnane R J and Elsner J B 2012 Maximum wind speeds and US hurricane losses *Geophys. Res. Lett.* **39** L16707
Pu X, Chen Q, Zhong Q, Ding R and Liu T 2019 Influence of the North Pacific Victoria mode on western North Pacific tropical cyclone genesis *Clim. Dyn.* **52** 245–56
Rayner N A *et al* 2006 Improved analyses of changes and uncertainties in sea surface temperature measured *in situ* since the mid-nineteenth century: the HadSST2 dataset *J. Clim.* **19** 446–69
Tippett M K, Camargo S J and Sobel A H 2011 A Poisson regression index for tropical cyclone genesis and the role of large-scale vorticity in genesis *J. Clim.* **24** 2335–57
Vimont D, Wallace J and Battisti D 2003 The seasonal footprinting mechanism in the Pacific: implications for ENSO *J. Clim.* **16** 2668–75

Wang B and Murakami H 2020 Dynamic genesis potential index for diagnosing present-day and future global tropical cyclone genesis *Environ. Res. Lett.* **15** 114008

Wang Z, Han L, Zheng J, Ding R, Li J, Hou Z and Chao J 2021 Evaluation of the performance of CMIP5 and CMIP6 models in simulating the Victoria mode–El Niño relationship *J. Clim.* **34** 7625–44

Xie S-P and Philander S G H 1994 A coupled ocean-atmosphere model of relevance to the ITCZ in the eastern Pacific *Tellus A* **46** 340

Ying M, Zhang W, Yu H, Lu X, Feng J, Fan Y, Zhu Y and Chen D 2014 An overview of the China meteorological administration tropical cyclone database *J. Atmos. Ocean. Technol.* **31** 287–301

Zhan R, Wang Y and Ding Y 2022 Impact of the western Pacific tropical easterly jet on tropical cyclone genesis frequency over the western North Pacific *Adv. Atmos. Sci.* **39** 235–48

Zhao J, Zhan R, Wang Y and Xu H 2018 Contribution of the interdecadal Pacific oscillation to the recent abrupt decrease in tropical cyclone genesis frequency over the Western North Pacific since 1998 *J. Clim.* **31** 8211–24

Zhou C, Wu L, Wang C and Cao J 2024 Shifted relationship between the Pacific decadal oscillation and western North Pacific tropical cyclogenesis since the 1990s *Environ. Res. Lett.* **19** 014071